Energy & Environmental Science

Accepted Manuscript

ROYAL SOCIETY OF CHEMISTRY

www.rsc.org/ees

Journal Name RSCPublishing

ARTICLE

Cite this: DOI: 10.1039/x0xx00000x

Pyrite FeS_2 for High-rate and Long-life Rechargeable Sodium Batteries

Zhe Hu, Zhiqiang Zhu, Fangyi Cheng, Kai Zhang, Jianbin Wang, Chengcheng Chen, Jun Chen*

Received 00th January 2012,
Accepted 00th January 2012

DOI: 10.1039/x0xx00000x

www.rsc.org/

It is desirable to develop electrode materials for advanced rechargeable batteries with low cost, long life, and high-rate capability. Pyrite FeS_2 as an easy-obtained natural mineral has been already commercialized in primary lithium batteries, but encountered problems in rechargeable batteries with carbonate-based electrolytes due to the limited cycle life caused by the conversion-type reaction (FeS_2 + 4M → Fe + $2M_2S$ (M=Li or Na)). Herein, we demonstrate that FeS_2 microspheres can be applied in room-temperature rechargeable sodium batteries with only intercalation reaction by simultaneously selecting compatible $NaSO_3CF_3$/diglyme electrolyte and tuning the cut-off voltage to 0.8 V. A surprising high-rate capability (170 $mAh\cdot g^{-1}$ at 20 $A\cdot g^{-1}$) and unprecedented long-term cyclability (~90% capacity retention for 20000 cycles) has been obtained. We suggest that a stable electrically conductive layer-structured Na_xFeS_2 was formed during cycling, which enables the highly reversible sodium intercalation and deintercalation. Moreover, 18650-type sodium batteries were constructed exhibiting a high capacity of ~4200 mAh (corresponding to 126 $Wh\cdot kg^{-1}$ and 382 $Wh\cdot L^{-1}$) and a capacity retention of 97% after an initial 200 cycles at 4 A during charge/discharge. This shows that the production of rechargeable sodium batteries with FeS_2 microspheres is viable for commercial utilization.

Introduction

There are ever growing demand of electric energy storage (EES) devices with rechargeable batteries that cover diverse applications ranging from portable electronics to electrical vehicles and smart grids.[1-8] Although rechargeable lithium-ion batteries (LIBs) have gained huge commercial success during the past two decades,[3, 9-17] expectation for large-scale market penetration raises much concern of supply limits and extraction costs of the elements in battery materials.[18] Alternatively, much effort has recently dedicated to sodium ion batteries (SIBs),[19, 20] which offer advantages of low cost, wide distribution, and inexhaustible resources.[21, 22] However, like that in LIBs, most electrode materials investigated for SIBs are still based on transition-metal oxides,[23-25] and generally showed lower energy output and inferior cyclability, mainly due to larger molecular mass and Na^+ ion radius. It remains challenging to exploit abundant Na-host materials that adopt robust structures with low cost, high capacity, fast charge/discharge, and long cycling life and to optimize the battery technology for fufilling better performance.

Being cheap and environmentally benign, pyrite FeS_2 has been applied in commercial primary Li/FeS_2 batteries.[26] Unfortunately, the poor cyclability of FeS_2 seriously hinders its application in rechargeable batteries.[27-29] It is reported that the intercalation (Equation 1) and conversion-type reaction (Equation 2) coexists at the first cycle.[30, 31] Generally, the latter reaction brings severe volume change to the electrode materials and sluggish kinetics for the reconstruction of FeS_2 at charge process, resulting in the inferior cyclic performance.[32] Even worse, it is difficult to control the reaction stage to avoid the detrimental conversion reaction through cutting off voltage since these two reactions share almost the same voltage platform.

$$FeS_2+xLi^++xe^-\rightarrow Li_xFeS_2\ (0<x<2,\ 1.5\sim1.7\ V) \quad (1)$$

$$Li_xFeS_2+(4-x)Li^++(4-x)e^-\rightarrow Fe+2Li_2S\ (\sim1.5\ V) \quad (2)$$

FeS_2 is also interesting in SIBs. Kim et al. firstly employed natural pyrite (FeS_2, Chile) in FeS_2/Na battery but the capacity decreased rapidly from ~630 to ~85 $mAh\cdot g^{-1}$ after 30 cycles.[33] Meanwhile, recent research has proved that commonly used ester-based electrolytes were not proper for Na/FeS_2 batteries since they would provoke side reaction with the anionic group.[34, 35] Thus, to enhance the cycling performance, the above mentioned problems should be considered together with the large volume change during the conversion. Furthermore, Na_xFeS_2 (x<2) has been testified as the intermediate during the reduction of FeS_2, confirming that the intercalation reaction also exists in Na/FeS_2 batteries.[33, 36] This offers the possibility to use cutting off voltage to control the reaction type.

$$FeS_2+xNa^++xe^-\rightarrow Na_xFeS_2\ (x<2) \quad (3)$$

$$Na_xFeS_2+(4-x)Na^++(4-x)e^-\rightarrow Fe+2Na_2S\ (\text{below } 0.8V) \quad (4)$$

Here, we discovered that by adopting diglyme (DGM) as the electrolyte and applying the cut-off voltage to 0.8 V, room-temperature rechargeable Na/FeS_2 batteries can be cycled by Equation (3) without passing through Equation (4) for 20000 cycles with ~90% capacity retention. Furthermore, it also featured impressive rate performance, rendering a capacity of ~170 mAh·g^{-1} at an ultrahigh current density of 20 A·g^{-1}. The excellent electrochemical performance was originated from two main points. On one hand, phase change from FeS_2 to conductive layered Na_xFeS_2 occurred in the initial few cycles, enabling highly reversible intercalation reaction. On the other hand, the pseudocapacitance-type reaction endowed the batteries with unprecedented high-rate characteristics. More importantly, the attempt for commercial 18650 batteries also showed considerable performance: stable discharge capacity of 4200 mAh at 4 A·g^{-1} for 200 cycles, which ensured the possibility for this kind of room-temperature batteries in commercial utilization.

Experimental section

Synthesis of FeS_2 microspheres

In a typical synthesis, 2 mmol $FeSO_4·7H_2O$ was first dissolved in 30 mL of dimethylformamide (DMF) and 40 mL of ethylene glycol (EG). Then, 10 mmol urea and 12.5 mmol sublimed sulfur were added in sequence with continuous stirring. After that, the mixture was loaded into a 100 mL Teflon-lined autoclave with sealing and maintained at 180 °C for 12 h. The obtained suspension was centrifuged and the precipitate was washed thoroughly with water and absolute ethyl alcohol. The final product was dried at 110 °C for 10 h in vacuum.

Material Characterization

Powder X-ray diffraction (XRD, Rigaku MiniFlex600, Cu Kα radiation), field-emission scanning electron microscopy (SEM, JEOL JSM-7500F, 5 kV), and transmission electron microscopy (TEM, Philips Tecnai FEI, 200 kV) were used to characterize the structure and morphology of the as-prepared samples. Tapped density analyzer (JZ-7) was employed to measure the tapped density. Raman spectra were obtained on a confocal Raman microscope (DXR, Thermo-Fisher Scientific) with an argon-ion laser (λ=532 nm) in ambient air. X-ray photoelectron spectroscopy (XPS, Perkin Elmer PHI 1600 ESCA system) and X-ray absorption spectroscopy (XAS, Shanghai Synchrotron Radiation Facility (SSRF)) were used to evaluate the valence of Fe and S. The sample was protected at Ar atmosphere in the glove box. Fe k-edge (7120 eV) XAS was performed in BL14W1 beamline of SSRF. Powder samples were uniformly pasted onto a metal free tape (3M Scotch 810-R) in an argon atmosphere. The white beam of the bending magnet was monochromatized by a Si (111) double monochromator. The absorption spectra were collected using a transmission mode near the K-edge of Fe by stepping the Si (111) monochromator. Data management of X-ray Absorption Near Edge Spectroscopy (XANES) and Extended X-ray Adsorption Fine Spectroscopy (EXAFS) was conducted using software Ifeffit Athena and Artemis. In Athena, EXAFS r-space data were obtained from Fourier transformed (FT) of energy normalized k3-weighted XANES data, of which backgrounds and pre-edge were already removed.

Electrochemical Test

Electrochemical measurements were performed with CR2032 coin-type cells. The working electrode was fabricated by mixing the as-prepared FeS_2, KS-6, and CMC-Na and SBR (solution in water, 20 mg·mL^{-1}) in the weight ratio of 8:1:0.4:0.6 by using water as a solvent. The slurry was then pasted onto a copper foil, and dried at 110 °C for 10 h in vacuum. Glass fiber and sodium foil were employed as the separator and anode, respectively. Different kinds of electrolyte were used: (1) 1 M sodium trifluomethanesulfonate ($NaSO_3CF_3$) in diglyme (DGM), (2) 1 M sodium perchlorate ($NaClO_4$) in DGM, (3) 1 M $NaSO_3CF_3$ in propylene carbonate (PC), and (4) 1 M $NaSO_3CF_3$ in ethylene carbonate and diethyl carbonate (EC-DEC, 1:1, m:m). The coin cells were assembled in an argon-filled glove box (Mikrouna Universal 2440/750). Galvanostatic tests were cycled between 0.1−3.0 and 0.8−3.0 V by using the LAND-CT2001A battery-testing instrument. Cyclic voltammograms (CVs) were performed between 0.8−3.0 V on Parstat 263A electrochemical workstation (AMETEK). Electrochemical impedance spectroscopy (EIS) was collected on Parstat 2273 electrochemical workstation (AMETEK). The ac perturbation signal was ±5 mV and the frequency ranged from 100 mHz to 100 kHz.

Assembling 18650-type Battery

The cathode electrode was fabricated by mixing FeS_2 (95%, 50μm), carbon black, and polyvinylidene fluoride (PVDF) in NMP. The slurry was spread onto Ni foam by medical blade and then dried in the vacuum oven. The electrode was pressed under 15MPa and was weighed. Na was pressed onto Ni foam and was employed as the anode. The battery was assembled by stacking the electrodes (two cathode electrodes, two anode electrodes, and three separators are stacked in the way of cathode/separator/anode). The electrolyte was 1 mol/L $NaSO_3CF_3$/DGM and Celgard 2340 was the separator. The electrochemical performance of 18650-type battery (ϕ18mm×H65mm, 50g) was assembled in the humidity-control working room (≤ 3.0%) and was tested by galvanostatic equipment using LAND-CT2001A battery-testing instrument. The tested current was 4 A and the voltage range was 0.9−3.0 V. To get the reliable data, the result was summarized by repeated tests.

Result

Phase and morphology characterization

FeS_2 microspheres were synthesized from a simple solvothermal route and commercial bulk FeS_2 powders were employed as an attempt for comparison. Fig. 1a shows the X-ray diffraction (XRD) of the two samples, both displaying high purity phase (standard FeS_2, JCPDS Card No. 42-1340). The

as-prepared FeS_2 presents the shape of microspheres that consist of tightly aggregated nanoparticles (~200 nm) shown in Fig. 1b, while the commercial FeS_2 shows the average particle size of 10 μm (Fig. 1c). The tapped density of FeS_2 microspheres and commercial FeS_2 is 2.2 $g\cdot cm^{-3}$ and 3.0 $g\cdot cm^{-3}$ (versus $LiCoO_2$ of 2.6 $g\cdot cm^{-3}$, Ref. 37), respectively (detailed method shown in supporting information).

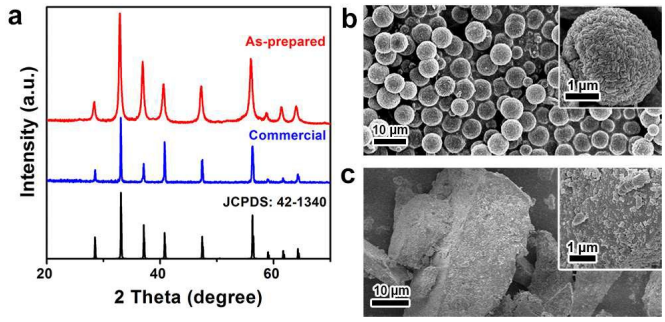

Fig. 1 Phase and morphology characterization of pyrite FeS_2. (a) XRD patterns of prepared and commercial FeS_2. Scanning electron microscopy (SEM) images of (b) as-prepared FeS_2 microspheres and (c) commercial FeS_2. Inset: surface morphology.

Optimization of electrolyte and voltage range

In order to obtain superior performance of FeS_2 electrode, two parameters, namely, the selected electrolyte and the cut-off discharge voltage are under consideration. Fig. 2a-d displays the charge and discharge curves of typical ester-based and ether-based electrolytes. It should be pointed out that the cells with DGM possess smaller voltage polarization and larger capacity. From the cyclic data, the electrolytes have prominent difference on the cycling performance (Fig. 2e). Specifically, $NaSO_3CF_3$/DGM possesses no obvious capacity fading from the second cycle and the stable discharge capacity was ~250 $mAh\cdot g^{-1}$. In contrast, $NaClO_4$/DGM performs comparable cyclability, rendering a capacity of ~240 $mAh\cdot g^{-1}$ without capacity fade for 60 cycles at 0.2 A g^{-1}. Carbonate-based electrolytes such as $NaSO_3CF_3$/PC and $NaSO_3CF_3$/EC-DEC suffer from large voltage polarization and induce rapid capacity decay (212 and 210 $mAh\cdot g^{-1}$ at 2nd cycle; 90 and 45 $mAh\cdot g^{-1}$ at 60th cycle, respectively). This is in good accordance with previous results since the electrolyte would react with anionic group.[35] We then calculated the apparent activation energy (E_a) of $NaSO_3CF_3$/DGM, $NaClO_4$/DGM, $NaSO_3CF_3$/PC, and $NaSO_3CF_3$/EC from the EIS data and Arrhenius equation (details shown in the supplementary information, Fig. S1).[38, 39] The corresponding values from Fig. 2f are 21.6, 26.9, 31.0, and 32.1 $kJ\cdot mol^{-1}$, respectively. These results indicate that the combination of $NaSO_3CF_3$ and DGM contributes to the best electrochemical performance in the measured system.

It should be pointed out that the cutting-off voltage also plays a key role in achieving such good cyclability. The capacity seriously fades from 780 to 100 $mAh\cdot g^{-1}$ within 50 cycles at 0.2 $A\cdot g^{-1}$ in the voltage range of 0.1–3 V (Fig. S2a,b). This is ascribed to the huge volume change caused by the conversion-type reaction and further proved by the observed FeS and Fe in the HRTEM images (Fig. S3). However, by tuning the cut-off voltage to 0.8 V, the cycling performance has been significantly enhanced. This result supports our idea that highly reversible intercalation reaction is realized by controlling the cut-off voltage.

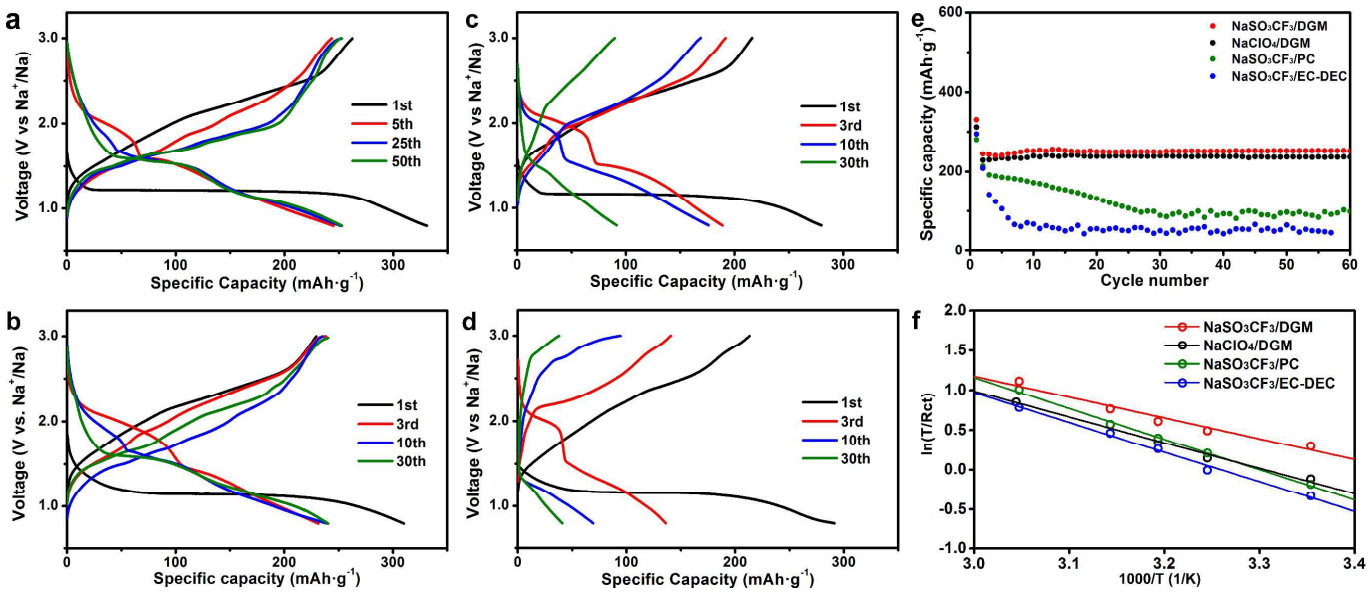

Fig. 2 Electrolyte optimization of Na/FeS_2 batteries. Discharge/charge curves at the current density of 0.2 $A\cdot g^{-1}$ in (a) $NaSO_3CF_3$/DGM, (b) $NaClO_4$/DGM, (c) $NaSO_3CF_3$/PC, and (d) $NaSO_3CF_3$/EC-DEC. (e) Cyclability in different electrolytes. (f) Apparent energy calculation: the relationship between $\ln(T/R_{ct})$ and 1000/T. Electrolyte solvent denotation: PC–propylene carbonate, EC–ethylene carbonate, DEC–diethyl carbonate.

Electrochemical performance

With the optimized test parameters, the electrochemical performance of CR2032 coin-type cells with FeS_2 microspheres as the cathode was further investigated. Surprisingly, the most appealing thing is the unbelievable cyclability (Fig. 3a). After a few cycles of activation as well as an initial irreversible capacity loss (Fig. S4a-c), the FeS_2 electrodes show almost no degradation for the next 20000 cycles with a high coulombic efficiency of nearly 100% at 1 $A\cdot g^{-1}$. Furthermore, a cycle life exceeding 12000 cycles is also obtained even at a high current density of 20 $A\cdot g^{-1}$. To our knowledge, such cycling performance is superior to that of any reported Na batteries which typically sustain at most several hundreds of cycles.[22] Meantime, the FeS_2 electrode also exhibits remarkable high-rate capability (Fig. 3b). A capacity of 170 $mAh\cdot g^{-1}$ (equivalent to 374 $mAh\cdot cm^{-3}$) is delivered even at an extremely high current density of 20 $A\cdot g^{-1}$, which permits full discharging/charging in less than one minute. Although such rates are achieved by supercapacitors,[40, 41] they are scarcely observed in lithium-ion batteries,[42] and have never been reported for Na systems. Ragone plots of the as-prepared FeS_2, together with representative layered oxides and polyanionic compounds are shown in Fig. S4d. Although the specific energy is slightly lower, the specific power of 23,000 $W\cdot kg^{-1}$ is one order of magnitude higher than that of typical materials in LIBs.[23, 43-45] In addition, the Na/FeS_2 cell can also operate at rough conditions. Fig. 3c shows typical discharge/charge curves (1 $A\cdot g^{-1}$) operated at −50, 25, and 50 °C with the specific capacities of 150, 205, and 275 $mAh\cdot g^{-1}$, respectively. Excellent cyclic stability with high capacity retention of 89.2% (at −50°C) and 98.8% (at 50°C) is obtained (Fig. S5). This should fulfill the commercial demands for wide application in special circumstances. The promotion on the electrochemical performance is due to the high purity of the as-prepared FeS_2 and the optimization of electrode preparation. In the previous work (Ref. 46), the impurities (Co, Ni, As, Te, Ge, etc.) existed in natural ore and the none-optimized electrode configuration (such as only 50% active material, excess non-conductive binder (25%) and inappropriate Al current collector) have bad influence on the cyclic property.

The intrinsically stability of Na/FeS_2 battery is further confirmed by using commercially available bulk FeS_2 powders as the cathode. The charge and discharge curves are very similar with the as-prepared FeS_2 microspheres (Fig. S6a). After a few cycles activation, the discharge capacity maintains ~180 $mAh\cdot g^{-1}$ at 1 $A\cdot g^{-1}$. Excitingly, the sustainable cyclability can still last for over thousands times at 1 $A\cdot g^{-1}$ as shown in Fig. 3d. The rate property was also measured (Fig. S6b). Although the bulk FeS_2 cannot be as excellent as the as-prepared FeS_2 microspheres, it can also achieve the high capacity of 120 $mAh\cdot g^{-1}$ at 10 $A\cdot g^{-1}$, which means that the whole batteries can be fully charged within one minute.

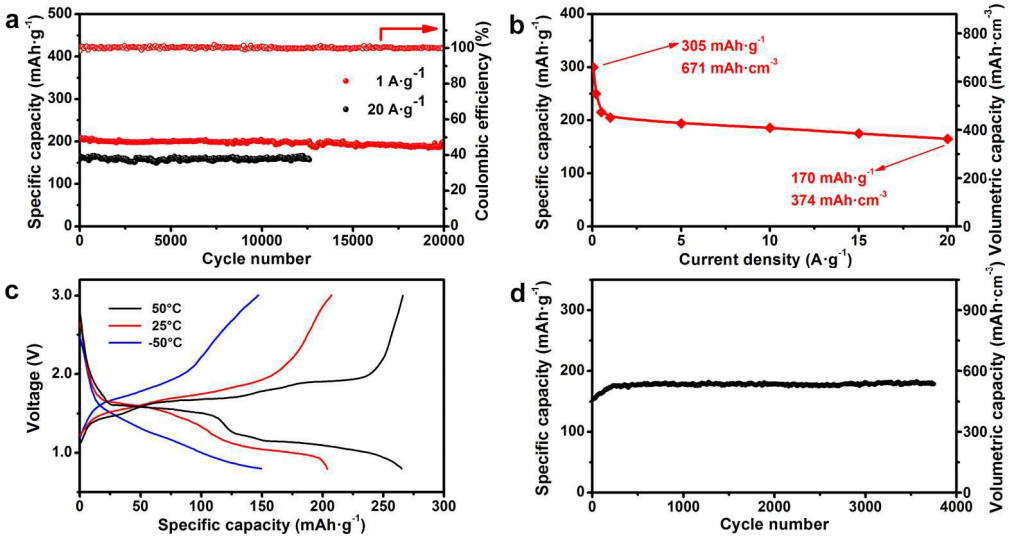

Fig. 3 Electrochemical performances of Na/FeS_2 cells with the optimized test parameters. (a) Cyclic performance of FeS_2 microspheres (same discharge/charge rate). (b) Rate capability of FeS_2 microspheres. (c) Charge-discharge profiles of as-prepared FeS_2 at 1 $A\cdot g^{-1}$ at different temperatures. (d) Cycling performance of commercial bulk FeS_2 coin cell at current density of 1 $A\cdot g^{-1}$.

Kinetics characterization

We have further diagnosed the electrode process kinetics of Na/FeS_2 cells with FeS_2 microspheres using electrochemical impendence spectroscopy (EIS). The Nyquist plot in Fig. 4a shows that at 1st cycle, the charge transfer resistance decreases significantly as discharge/charge proceeds, which is attributed to the formation of a conducive intermediate. Only small changes were found in the curves at 50th cycle (Fig. 4b). There is a profound difference between the phase angles at the 1st and the 50th cycle. The more vertical line (i.e., close to 90° phase angle) shown in the latter indicates a capacitive behavior.[47, 48] This is also evidenced by the analysis of cyclic voltammetry (CV, Fig. 4c). CV curves and kinetic information demonstrate that a combination of capacitive process and diffusion-limited redox reaction manages the electrochemical reaction. A 46%

fraction of the total charge comes from capacitive processes (Fig. 4d, detailed method shown in Fig. S7), which accounts for the unprecedented high rate and long cycling performance of Na/FeS_2 cells. This capacitive behavior is similar to the case of metal oxides and metal dichalcogenides.[48, 49]

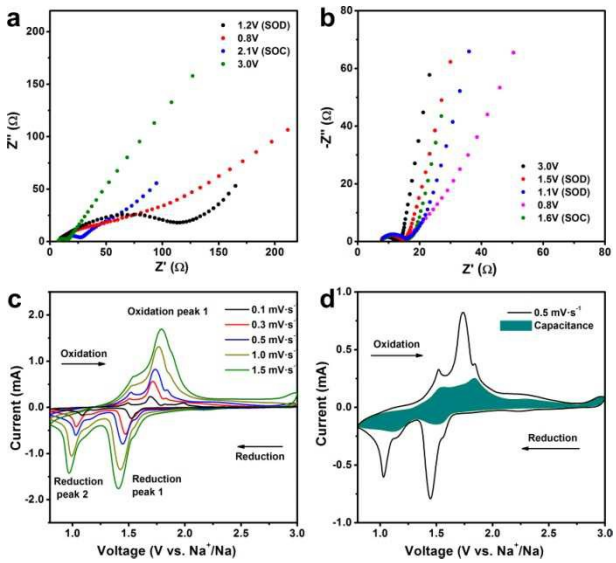

Fig. 4 Kinetics characterization of Na/FeS_2 cells with the optimized test parameters. Nyquist plots of the impedance (a) at the first and (b) at the fiftieth cycles. SOD/SOC: state of discharge/charge. (c) Cyclic voltammogram of the cell cycling for 500 times in different sweep rates. (d) Cyclic voltammogram with the capacitive contribution to the total current shown by the shaded region. Results correspond to the cells with FeS_2 microspheres.

Electrochemical reaction mechanism

We also performed a series of structural characterizations to study the mechanism of Na/FeS_2 cell during cycling. Fig. 5a displays the typical galvanostatic profiles at the first (I→II→III→IV→V) and the fiftieth cycle (VI→VII→VIII→IX). The initial profile presents a flat plateau at 1.2 V with high charge-discharge polarization. This behavior, as observed in the Li/FeS_2 system,[27-29] could be explained by phase change. Fig. 5b shows the XRD patterns of the selected states. During discharge process in the first cycle (I→III), the characteristic peaks of FeS_2 gradually disappear and a peak around 31° comes out, which could be assigned to a monoclinic $NaFeS_2$ phase (JCPDS Card No. 34-935). As no characteristic peaks of FeS_2 are found in the XRD patterns at state V, the final charge product should be monoclinic Na_xFeS_2 (x approaching to 0.2). From the 2nd cycle, the discharge/charge curves change all the time because of the gradual phase transformation, and finally the curves tend to be stable at the 50th cycle. Accordingly, the XRD peak at 31° gradually shifts to 29°. Meanwhile, the characteristic peak at 26.2° is assigned to KS-6 (graphite, the conductive agent). Rietveld refinement of the patterns collected at state VIII indicates the formation of a layered compound of trigonal Na_xFeS_2 with x around 1.6 (Fig. S8). This means that the theoretical specific capacity is 357 $mAh\cdot g^{-1}$ for Na/FeS_2 batteries cycling between 0.8–3.0 V. Since the discharge/charge curves were nearly kept without change after 50 cycles, we conclude that since then the layered structures could well maintain within the selected potential window (i.e., 0.8–3.0 V), enabling the highly reversible intercalation reaction. The final charge product should be Na_xFeS_2 with x around 0.2. Results from high resolution transmission electron microscopy (HRTEM, Fig. 5c and Fig. S9) and selected-area electron diffraction (SAED, Fig. 5d) show that the clear lattice fringe of 0.29 nm at II, III, IV, and V, turns to be 0.31 nm at VI, VII, VIII, and IX, corresponding to the phase change from monoclinic to trigonal system. This result fits well with the XRD data.

Journal Name RSCPublishing

ARTICLE

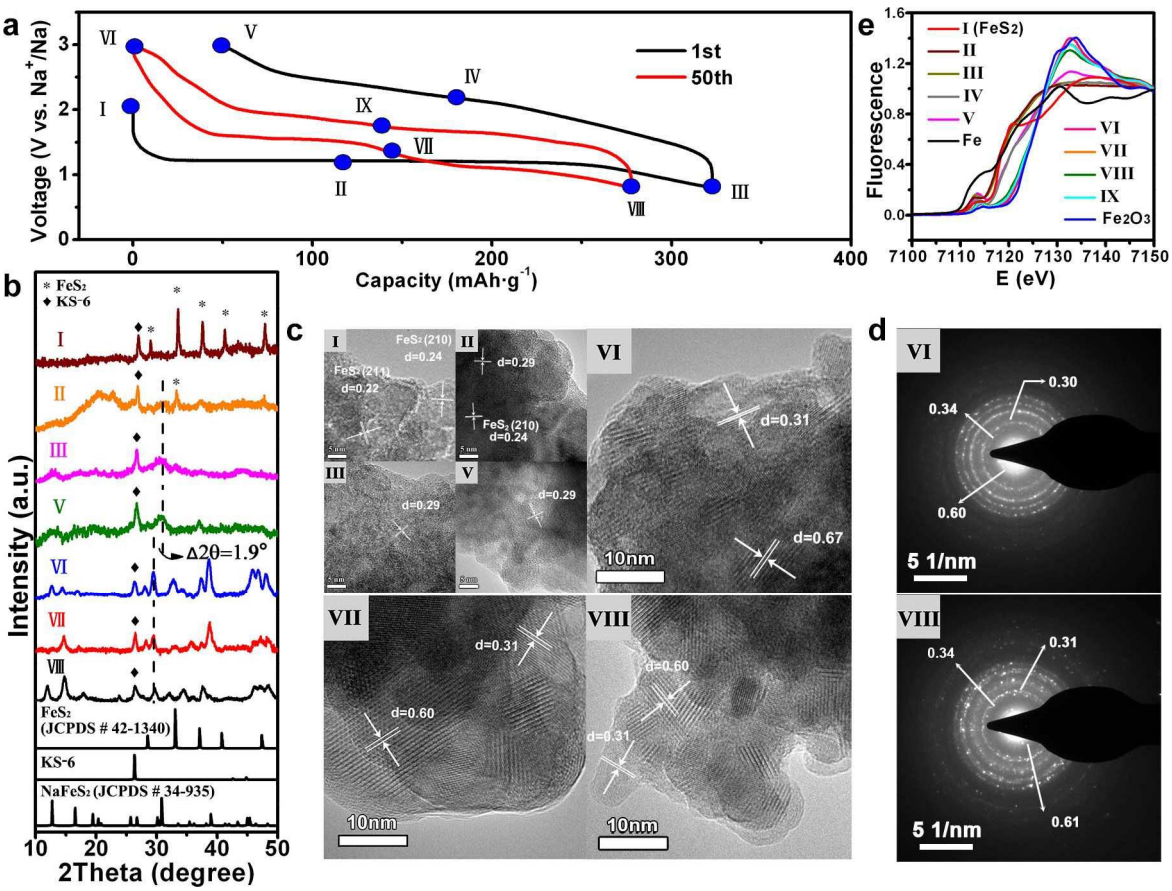

Fig. 5 Structural evolution of FeS_2 during electrochemical reaction with sodium. (a) Cut-off voltage-dependent discharge and charge curves at the first and fiftieth cycle. The marked points are analyzed *ex situ* after dismantling the cells. (b) Collected XRD profiles of and standard FeS_2 (JCPDS Card No. 42-1340) and $NaFeS_2$ (JCPDS Card No. 34-935). (c) TEM images. (d) SAED patterns. The marks (I→IX) in (b,c,d,e) correspond to the marks in (a). (e) Synchrotron X-ray absorption spectroscopy of the electrodes at different cycled states and the reference Fe and Fe_2O_3.

In addition to structural evolution, the oxidation state of cycled species needs to be clarified as both Fe and S are redox reactive elements. During the initial cycle (I→II→III→IV→V), our measurements of synchrotron X-ray absorption spectroscopy (XAS, Fig. 5e) reveal that the Fe valence is similar in both FeS_2 and discharged species (II and III) but increases slightly to a multivalent state on charging (IV and V). After activation (VI, VII, VIII, and IX), the oxidation state of Fe remains almost unchanged, presenting a valence close to Fe^{3+}. Instead, X-ray photoelectron spectroscopy (XPS, Fig. S10) evidences that the reversible redox reactions of FeS_2 electrode proceed through unusual valence change of sulfur.[50]

The evolution of Na/FeS_2 batteries was recorded by the ex-situ SEM and TEM method. Fig. S11 shows the SEM and HRTEM images at different cycles. It can be seen that the pure FeS_2 nanoplates gradually become larger on the surface of the microspheres at 50th cycle, presumably the layered structured Na_xFeS_2. These changes were also found in Li/FeS_2, and the plat-cluster was assigned to be $Li_{2.06}FeS_2$.[26] After 20000 cycles, the microspheres crack into individual plate. This also explains the capacity fade during such long cycles. We also measured the XRD and HRTEM images at 0.8 V and 3.0 V of the Na/FeS_2 batteries after cycling for 20000 cycles (Fig. S12). From XRD results, the crystallinity of the active materials tends to become weaker, but the typical peaks at ~29° still can be detected and the d-space of 0.31 nm can also be measured in the HRTEM images, which means that the phase can be maintained after cycling. From the above mentioned characterization, we observe that the nanoplates become larger together with the phase change from monoclinic to trigonal system. Finally, the microspheres pulverize into small pieces

and the tendency of well-crystallized Na_xFeS_2 to weak-crystallized leads to the capacity fade.

Commercial 18650 batteries

To verify the possibility of Na/FeS_2 for commercial application, 18650-type batteries based on this system are fabricated. Fig. 6 presents the charge and discharge curves and cyclic performance of the assembled cells. A stable discharge capacity of 4200 mAh with an average potential of ~1.5 V is obtained (126 $Wh\cdot kg^{-1}$ and 382 $Wh\cdot L^{-1}$). The reversible capacity can last for 200 cycles with 97% capacity retention. It should be pointed out that the specific energy of the proposed Na/FeS_2 system is comparable to the common lithium ion batteries (75−160 $Wh\cdot kg^{-1}$).[51] For the MODEL S of Tesla, each battery of 18650-type holds the capacity of about 3100 mAh.[52] Thus, present Na/FeS_2 battery should have interest. The active material FeS_2 is very cheap and easily obtained from the earth, which makes it favorable for the commercial electric energy storage utilizations. Certainly, further investigation like the safeguard procedures should be concerned in practical applications.

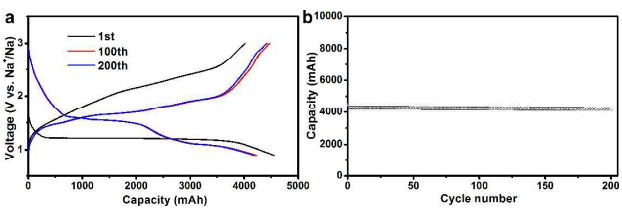

Fig. 6 (a) Charge-discharge curves and (b) cycling performance of 18650-type battery at a current density of 4 A in the voltage range from 0.9−3 V.

Discussion

The above investigations now yield an overall picture of the structure optimization mechanism of Na/FeS_2 cells with the selected $NaSO_3CF_3$/diglyme electrolyte and the cut-off voltage of 0.8 V. On one hand, the electrolyte affects the electrochemical properties on two aspects: the solvent-salt stability and reaction energy barrier. Carbonate-based electrolyte, as reported, would react with anionic group, leading to capacity decay. However, no such problem occurs in ether-based electrolyte, thus guaranteeing the long-term cyclability. In addition, solvent-salt interactions decide the steric hindrance by the coordination environment (carbonate or ether group coordinates to Na^+ ions Ref. 53, which are detected by the Raman shifts among solvent, salt, and solvent-salt solution shown in Fig. S13, Ref. 54) The Na-carbonate group suffers from ponderous volume, exhibiting inevitable obstruction and sluggish kinetics during the electrochemical reaction, as shown in Fig. 7. On the contrary, selected DGM possesses the 1D flexible chain morphology. Swift intercalation with smaller reaction energy barrier would enhance the reaction kinetics between Na-DGM and active electrode material. On the other hand, referring to the cut-off voltage, there are two processes existing: activation process and reversible intercalation. During the starting a few cycles, there is a gradual phase change from FeS_2 to layered Na_yFeS_2. Then reversible intercalation of sodium ions takes place between the layered sulfide species: Na_yFeS_2 ($y\approx0.2$, charge state) and Na_yFeS_2 ($y\approx1.6$, discharge state), presenting the high capacity retention of 90% after 20000 cycles. Moreover, the DFT calculation affirms the change from semi-conductive FeS_2 to the metallic-type conductive Na_xFeS_2 (Fig. S14), which is an explanation for the superior rate performance. In all, by ensuring DGM as the optimized electrolyte and controlling the terminate voltage to 0.8V, the phase change, ultrasmall particle size, and solvent-salt collaboration insure the redox and capacitive behavior of Na/FeS_2 battery.

Journal Name RSCPublishing

ARTICLE

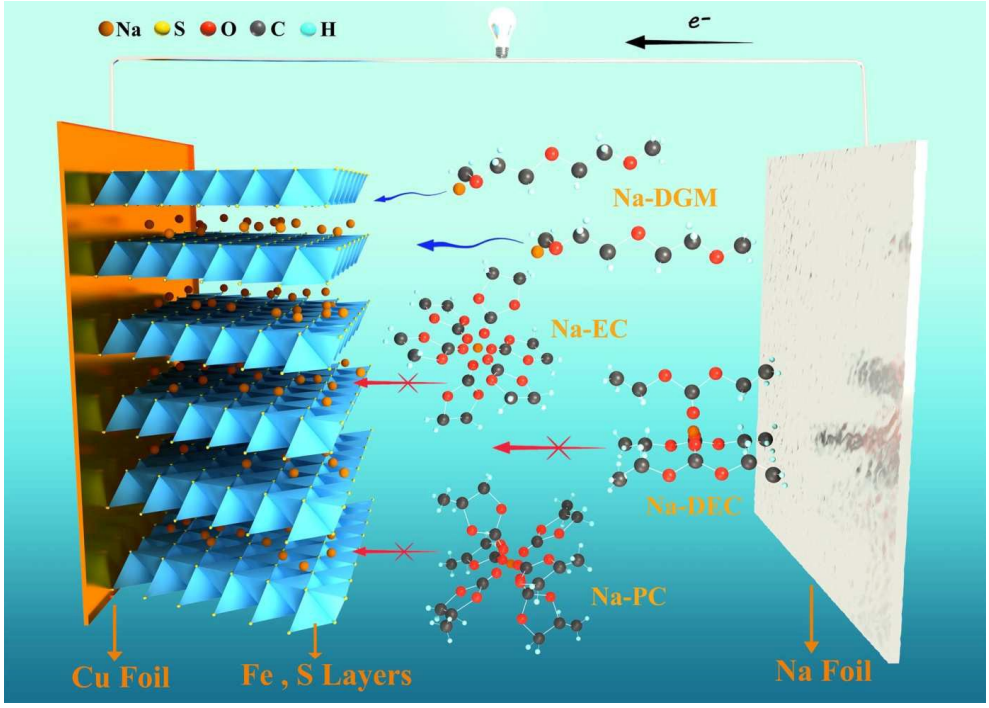

Fig. 7 Schematic illustration of the operation mechanism of iron sulfides in Na/FeS_2 cells.

Conclusion

This study highlights the importance of electrolyte selection and voltage control in improving the performance of rechargeable Na/FeS_2 cells. By tuning these factors, the combination of pseudocapacitance and redox reactions in iron sulfides is feasible to permit Na storage with unexpected high rate capability and durable cyclability. The capacity can reach 170 mAh·g^{-1} at 20 A·g^{-1} and the cell cycling at 1 A·g^{-1} achieves high capacity retention of ~90% after 20000 cycles. Moreover, commercial-type 18650 battery has been successfully fabricated, showing the capacity of 4200 mAh and considerable energy density of 126 Wh·kg^{-1} and 382 Wh·L^{-1} per unit cell. These results show that rechargeable Na/FeS_2 batteries are potential applications in the area of electric vehicles and smart grids.

Acknowledgements

We acknowledge support from State Key Project of Fundamental Research for Nanoscience and Nanotechnology (grant No. 2011CB935900), National Science Foundation of China (NSFC, grant No. 21322101 and 21231005), and Ministry of Education (grant No. B12015, 113016A and ACET-13-0296).

Notes and references

Key Laboratory of Advanced Energy Materials Chemistry (Ministry of Education), Collaborative Innovation Center of Chemical Science and Engineering, Nankai University, Tianjin, 300071, People's Republic of China. Fax: +86-22-23509571; Tel: +86-22-23506808; E-mail: chenabc@nankai.edu.cn

†Electronic Supplementary Information (ESI) available: HRTEM images, additional electrochemical characterization, Nyquist plots, capacitance calculation, computational details, XRD refinement, XPS data and Raman spectra. See DOI: 10.1039/b000000x/

References:

1. M. Armand and J. M. Tarascon, *Nature*, 2008, **451**, 652.
2. J. B. Goodenough and K. S. Park, *J. Am. Chem. Soc.*, 2013, **135**, 1167.
3. Z. Wang, D. Luan, S. Madhavi, Y. Hu and X. W. Lou, *Energy Environ. Sci.*, 2012, **5**, 5252.
4. B. Scrosati, J. Hassoun and Y.-K. Sun, *Energy Environ. Sci.*, 2011, **4**, 3287.
5. O. K. Park, Y. Cho, S. Lee, H.-C. Yoo, H.-K. Song and J. Cho, *Energy Environ. Sci.*, 2011, **4**, 1621.
6. V. Etacheri, R. Marom, R. Elazari, G. Salitra and D. Aurbach, *Energy Environ. Sci.*, 2011, **4**, 3243.
7. Y. Wang, P. He and H. Zhou, *Energy Environ. Sci.*, 2011, **4**, 805.

8. F. Y. Cheng, J. Liang, Z. L. Tao and J. Chen, *Adv. Mater.*, 2011, **23**, 1695.
9. M. S. Whittingham, *Chem. Rev.*, 2004, **104**, 4271.
10. P. G. Bruce, S. A. Freunberger, L. J. Hardwick and J.-M. Tarascon, *Nat. Mater.*, 2012, **11**, 19.
11. M. S. Islam and C. A. J. Fisher, *Chem. Soc. Rev.*, 2014, **43**, 185.
12. Y. Lu, Z. Tu and L. A. Archer, *Nat. Mater.*, 2014, **13**, 961.
13. B. L. Ellis, W. R. M. Makahnouk, Y. Makimura, K. Toghill and L. F. Nazar, *Nat. Mater.*, 2007, **6**, 749.
14. K. Zhang, X. Han, Z. Hu, X. Zhang, Z. Tao and J. Chen, *Chem. Soc. Rev.*, 2015, DOI: 10.1039/c4cs00218k.
15. D.-L. Ma, Z.-Y. Cao, H.-G. Wang, X.-L. Huang, L.-M. Wang and X.-B. Zhang, *Energy Environ. Sci.*, 2012, **5**, 8538.
16. H. Wang, Y. Yang, Y. Liang, G. Zheng, Y. Li, Y. Cui and H. Dai, *Energy Environ. Sci.*, 2012, **5**, 7931.
17. F. Cheng, H. Wang, Z. Zhu, Y. Wang, T. Zhang, Z. Tao and J. Chen, *Energy Environ. Sci.*, 2011, **4**, 3668.
18. C. Wadia, P. Albertus and V. Srinivasan, *J. Power Sources*, 2011, **196**, 1593.
19. S. Wang, L. Wang, Z. Zhu, Z. Hu, Q. Zhao and J. Chen, *Angew. Chem. Int. Ed.*, 2014, **126**, 6002.
20. H. Pan, Y.-S. Hu and L. Chen, *Energy Environ. Sci.*, 2013, **6**, 2338.
21. V. Palomares, P. Serras, I. Villaluenga, K. B. Hueso, J. Carretero-Gonzalez and T. Rojo, *Energy Environ. Sci.*, 2012, **5**, 5884.
22. M. D. Slater, D. Kim, E. Lee and C. S. Johnson, *Adv. Funct. Mater.*, 2013, **23**, 947.
23. N. Yabuuchi, M. Kajiyama, J. Iwatate, H. Nishikawa, S. Hitomi, R. Okuyama, R. Usui, Y. Yamada and S. Komaba, *Nat. Mater.*, 2012, **11**, 512.
24. M. Guignard, C. Didier, J. Darriet, P. Bordet, E. Elkaïm and C. Delmas, *Nat. Mater.*, 2013, **12**, 74.
25. Y. Sun, L. Zhao, H. Pan, X. Lu, L. Gu, Y.-S. Hu, H. Li, M. Armand, Y. Ikuhara, L. Chen and X. Huang, *Nat. Commun.*, 2013, **4**, 1870.
26. Y. Shao-Horn, S. Osmialowski and Q. C. Horn, *J. Electrochem. Soc.*, 2002, **149**, A1499.
27. D. Golodnitsky and E. Peled, *Electrochim. Acta*, 1999, **45**, 335.
28. T. A. Yersak, H. A. Macpherson, S. C. Kim, V.-D. Le, C. S. Kang, S.-B. Son, Y.-H. Kim, J. E. Trevey, K. H. Oh, C. Stoldt and S.-H. Lee, *Adv. Energy Mater.*, 2013, **3**, 120.
29. R. Fong, J. R. Dahn and C. H. W. Jones, *J. Electrochem. Soc.*, 1989, **136**, 3206.
30. C. H. W. Jones, P. E. Kovacs, R. D. Sharma and R. S. McMillan, *J. Phys. Chem.*, 1991, **95**, 774.
31. J. Liu, Y. Wen, Y. Wang, P. A. van Aken, J. Maier and Y. Yu, *Adv. Mater.*, 2014, **26**, 6025.
32. D. Zhang, Y. J. Mai, J. Y. Xiang, X. H. Xia, Y. Q. Qiao and J. P. Tu, *J. Power Sources*, 2012, **217**, 229.
33. T. B. Kim, J. W. Choi, H. S. Ryu, G. B. Cho, K. W. Kim, J. H. Ahn, K. K. Cho and H. J. Ahn, *J. Power Sources*, 2007, **174**, 1275.
34. Y.-X. Yin, S. Xin, Y.-G. Guo and L.-J. Wan, *Angew. Chem. Int. Ed.*, 2013, **52**, 13186.
35. J. Gao, M. A. Lowe, Y. Kiya and H. D. Abruña, *J. Phys. Chem. C*, 2011, **115**, 25132.
36. Z. Shadike, Y.-N. Zhou, F. Ding, L. Sang, K.-W. Nam, X.-Q. Yang and Z.-W. Fu, *J. Power Sources*, 2014, **260**, 72.
37. Y. K. Sun, S. M. Oh, H. K. Park and B. Scrosati, *Adv. Mater.*, 2011, **23**, 5050.
38. H. Gao, Z. Hu, K. Zhang, F. Cheng and J. Chen, *Chem. Commun.*, 2013, **49**, 3040.
39. H. Ma, S. Zhang, W. Ji, Z. Tao and J. Chen, *J. Am. Chem. Soc.*, 2008, **130**, 5361.
40. Y. Xu, Z. Lin, X. Zhong, X. Huang, N. O. Weiss, Y. Huang and X. Duan, *Nat. Commun.*, 2014, **5**, 4554.
41. P. Simon and Y. Gogotsi, *Nat. Mater.*, 2008, **7**, 845.
42. B. Kang and G. Ceder, *Nature*, 2009, **458**, 190.
43. D. Choi, D. Wang, V. V. Viswanathan, I.-T. Bae, W. Wang, Z. Nie, J.-G. Zhang, G. L. Graff, J. Liu, Z. Yang and T. Duong, *Electrochem. Commun.*, 2010, **12**, 378.
44. P. Gao, Y. Li, H. Liu, J. Pinto, X. Jiang and G. Yang, *J. Electrochem. Soc.*, 2012, **159**, A506.
45. K. Saravanan, C. W. Mason, A. Rudola, K. H. Wong and P. Balaya, *Adv. Energy Mater.*, 2013, **3**, 444.
46. Y. Wang, H. Liao, J. Wang, X. Qian, Y. Zhu and S. Cheng, *Int. J. Electrochem. Sci*, 2013, **8**, 4002.
47. P. Simon, Y. Gogotsi and B. Dunn, *Science*, 2014, **343**, 1210.
48. T. Brezesinski, J. Wang, S. H. Tolbert and B. Dunn, *Nat. Mater.*, 2010, **9**, 146.
49. Z. Hu, L. Wang, K. Zhang, J. Wang, F. Cheng, Z. Tao and J. Chen, *Angew. Chem. Int. Ed.*, 2014, **53**, 12794.
50. A. Kitajou, J. Yamaguchi, S. Hara and S. Okada, *J. Power Sources*, 2014, **247**, 391.
51. B. Dunn, H. Kamath and J. M. Tarascon, *Science*, 2011, **334**, 928.
52. Electric vehicles of Tesla use 18650 type batteries with $LiCoO_2$ as the cathode. For example, the MODEL S possess a total capacity of 85kWh, which is supplied by about eight thousands 18650-type batteries through complex assembling. Each battery holds the capacity of about 3100 mAh.
53. Z. Li, L. Yuan, Z. Yi, Y. Sun, Y. Liu, Y. Jiang, Y. Shen, Y. Xin, Z. Zhang and Y. Huang, *Adv. Energy Mater.*, 2014, **4**, 1301473.
54. A. Ponrouch, R. Dedryvere, D. Monti, A. E. Demet, J. M. Ateba Mba, L. Croguennec, C. Masquelier, P. Johansson and M. R. Palacin, *Energy Environ. Sci.*, 2013, **6**, 2361.

Table of contents

Figure (5.6 cm ×4.0 cm)

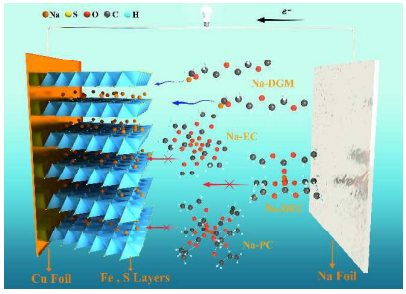

Text:

High-performance rechargeable Na/FeS_2 batteries with only intercalation reaction are obtained by selecting $NaSO_3CF_3$/diglyme electrolyte and tuning the cut-off voltage to 0.8 V.